The Three-Dimensional Structures of the *Mycobacterium tuberculosis* Dihydrodipicolinate Reductase−NADH−2,6-PDC and −NADPH−2,6-PDC Complexes. Structural and Mutagenic Analysis of Relaxed Nucleotide Specificity[†,‡]

Maurizio Cirilli,[§] Renjian Zheng, Giovanna Scapin,[||] and John S. Blanchard*

Department of Biochemistry, Albert Einstein College of Medicine, 1300 Morris Park Avenue, Bronx, New York 10461

Received February 19, 2003; Revised Manuscript Received May 20, 2003

ABSTRACT: Dihydrodipicolinate reductase (DHPR) catalyzes the reduced pyridine nucleotide-dependent reduction of the α,β-unsaturated cyclic imine, dihydrodipicolinate, to generate tetrahydrodipicolinate. This enzyme catalyzes the second step in the bacterial biosynthetic pathway that generates *meso*-diaminopimelate, a component of bacterial cell walls, and the amino acid L-lysine. The *Mycobacterium tuberculosis dapB*-encoded DHPR has been cloned, expressed, purified, and crystallized in two ternary complexes with NADH or NADPH and the inhibitor 2,6-pyridinedicarboxylate (2,6-PDC). The structures have been solved using molecular replacement strategies, and the DHPR−NADH−2,6-PDC and DHPR−NADPH−2,6-PDC complexes have been refined against data to 2.3 and 2.5 Å, respectively. The *M. tuberculosis* DHPR is a tetramer of identical subunits, with each subunit composed of two domains connected by two flexible hinge regions. The N-terminal domain binds pyridine nucleotide, while the C-terminal domain is involved in both tetramer formation and substrate/inhibitor binding. The *M. tuberculosis* DHPR uses NADH and NADPH with nearly equal efficiency based on V/K values. To probe the nature of this substrate specificity, we have generated two mutants, K9A and K11A, residues that are close to the 2′-phosphate of NADPH. These two mutants exhibit decreased specificity for NADPH by factors of 6- and 30-fold, respectively, but the K11A mutant exhibits 270% of WT activity using NADH. The highly conserved structure of the nucleotide fold may permit other enzyme's nucleotide specificity to be altered using similar mutagenic strategies.

L-Lysine and *meso*-diaminopimelate (DAP)[1] are synthesized in bacteria in a mechanistically complex, multistep sequence starting with L-aspartate (*1*). Two enzymes catalyze the conversion of L-aspartate to L-aspartate semialdehyde, a common precursor for the biosynthesis of L-threonine, L-isoleucine, L-methionine, and L-lysine. Dihydrodipicolinate synthase and dihydrodipicolinate catalyze the consecutive aldol condensation of pyruvate to L-aspartate semialdehyde to generate the α,β-unsaturated cyclic imine, dihydrodipicolinate (DHP), and reduction to form tetrahydrodipicolinate (THP). The conversion of THP to meso-DAP, and then to L-lysine is achieved via three different pathways in various bacterial species (*2*−*4*). *meso*-DAP is incorporated into the nucleotide sugar−pentapeptide precursor of bacterial peptidoglycan, and the D-amino acid center serves as the nucleophile in the carboxypeptidase-catalyzed cross-linking reaction in Gram-negative bacteria and mycobacteria. Inhibition of the biosynthesis of meso-DAP in *Mycobacterium smegmatis*, a fast growing, nonpathogenic species, has been shown to result in cell lysis (*6*), suggesting that enzymes in this pathway are novel targets for the development of broad spectrum antibacterial compounds.

Scheme 1: Reaction Catalyzed by Dihydrodipicolinate Reductase

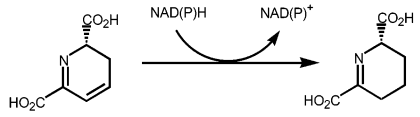

Dihydrodipicolinate reductase (DHPR, Scheme 1) catalyzes the pyridine nucleotide-dependent reduction of the α,β-unsaturated bond to generate tetrahydrodipicolinate (THP). The enzyme was initially identified in *E. coli* extracts (*7*), and its gene sequence was the first reported for any enzyme in the pathway (*8*). The *dapB* gene that encodes the reductase has been identified in numerous Gram-negative, Gram-positive, and archae bacterial species, in addition to mycobacteria (*9*). The *E. coli* enzyme has been mechanistically and structurally characterized in detail (*10*−*14*).

The molecular basis for nucleotide specificity in pyridine nucleotide-dependent dehydrogenases has been a focus of attention for over three decades. A number of studies have attempted to define or identify sequence "motifs" that would

[†] This work was supported by NIH Grant AI33696.

[‡] Coordinates have been deposited with the Brookhaven Data Bank with PDB accession numbers 1P9L and 1C3V for the DHPR−NADH−2,6-PDC and DHPR−NADPH−2,6-PDC complexes, respectively.

* To whom correspondence should be sent. (718) 430-3096. Fax: (718) 430-8565. E-mail: blanchar@aecom.yu.edu.

[§] Current address: Institute of Neurobiology and Molecular Medicine, CNR, via del Fosso del Cavaliere, 100, 00133 Rome, Italy.

[||] Current address: Merck Research Laboratories, P.O. Box 2000, RY50-105, Rahway, NJ 07065.

[1] Abbreviations: DHPR, the *dapB*-encoded dihydrodipicolinate reductase; NADH, β-nicotinamide adenine dinucleotide; NADPH, β-nicotinamide adenine dinucleotide 2′-phosphate; 2,6-PDC, 2,6-pyridine dicarboxylate; DAP, *meso*-diaminopimelate.

10.1021/bi030044v CCC: $25.00
Published on Web 08/16/2003

Table 1: Statistics for the Data Set Used in the Three-Dimensional Structure Determination and Refinement of the *M. tuberculosis* DHPR−NADH−2,6-PDC and DHPR−NADPH−2,6-PDC Complexes

data collection statistics	DHPR−NADH−2,6-PDC	DHPR−NADPH−2,6-PDC
resolution in Å (last shell)	25.0−2.3 Å (2.4−2.3)	30.4−2.4 (2.63−2.54)
number of Reflections	24,502[a] (2353)	16,553[a] (3306)
% of possible	98.5 (95.1)	87.6 (88.6)
number of observations	77,959 (4910)	64,913 (4962)
redundancy	3.2 (2.1)	3.3 (2.7)
$I/\sigma I$	13.6 (3.3)	7.1 (2.1)
R_{sym}	7.8 (20.6)	10.5 (39.5)
protein atoms	3,620[b]	3,620[b]
ligand atoms	125[c]	133[c]
solvent atoms	117	25
crystallographic *R*-factor (%)	19.3	19.6
free *R*-factor (%)	25.0	24.3
rms bond lengths (Å)/angles (deg)	0.011/1.63	0.007/1.32

[a] 97.1% of possible; 1 s cutoff on F has been applied during refinement. [b] Residues 1−245 for each of the two monomers in the asymmetric unit. Glu63 and Lys94 in MOL1 are present as alanines because of lack of electron density for the side chains. [c] One molecule of NAD(P)H and one molecule of 2,6-PDC per monomer, and one molecule of PEG200 per dimer.

have predictive capabilities. These have focused on the dinucleotide binding fold fingerprint (*15*) but have generally failed to provide a rule that can be used in a predictive fashion (*16*, *17*), although the preference for NADH or NAD^+ is correlated with the presence of a glutamate or aspartate residue at the end of the β1-α1-β2-fold (*17*, *18*) that hydrogen bonds to the adenosyl ribose 2′- and 3′-hydroxyl groups. Preference for NADPH or $NADP^+$ is similarly correlated with the presence of cationic residues in this same carboxyl terminal region, especially arginine, that make specific electrostatic stabilizing interactions with the 2′-phosphate monoester (*16*, *19*−*21*). The unusual dual pyridine nucleotide specificity exhibited by *E. coli* DHPR has been shown to be due to the presence of both an acidic (Glu38) and an adjacent basic (Arg39) residue in the adenosyl ribose binding pocket (*14*). Alignment of the *Escherichia coli* and *Myobacterium tuberculosis* DHPR amino acid sequences reveals significant differences in regions thought to confer nucleotide selectivity (*9*), specifically the replacement of the two residues, Glu38 and Arg39, shown to interact with the adenosyl ribose ring, by Asp33 and Ala 34. This suggested that the *M. tuberculosis* reductase would exhibit a more pronounced specificity for NADH as reductant. We report here the structures of the *M. tuberculosis* DHPR−NADH−2,6-PDC and DHPR−NADPH−2,6-PDC complexes and the kinetic characterization of the nucleotide specificity of the WT MtDHPR and two site-directed mutants.

EXPERIMENTAL METHODS

Cloning, Expression, and Purification of WT and K9A and K11A Mutants of M. tuberculosis DHPR. The published sequence of the *M. tuberculosis* d*apB* gene (*9*), encoding DHPR, was used to design PCR primers used to amplify the gene from genomic *M. tuberculosis* $H37R_v$ DNA. The oligonucleotides primers, 5′-TACATATGCGGGTAGGCGTC-CTTGG-3′ and 5′-CGGGATCCTTCAGTGCAGATCGAG-TAG-3′, contained NdeI and BamHI restriction sites, respectively. Amplification yielded a ca. 750 bp product that was digested with the two restriction enzymes, ligated into a similarly restricted pET23a(+) vector, and transformed into *E. coli* BL21(DE3). The K9A and K11A mutants were created by PCR as previously described (*22*), and both WT and mutant PCR gene products were sequenced (*23*) to confirm no unexpected mutations had been introduced during these procedures. The expression and purification of both enzymes, and the spectrophotometric determination of the kinetic parameters for pyridine nucleotide substrates were performed as previously reported (*10*).

Protein Crystallization and Data Collection. Orthorhombic crystals of the ternary complexes of *M. tuberculosis* DHPR−2,6-PDC−NADH/NADPH were obtained using the hanging drop vapor diffusion method. Crystals were grown at room temperature from 6 μL drops containing 3 μL of protein solution, containing 20 mg/mL DHPR, 2 mM NADH, or NADPH and 30 mM 2,6-PDC and 3 μL of precipitant solution (2.2 M ammonium sulfate in 0.1 M Hepes, pH 7.5, containing 3% PEG 400). Crystals in the shapes of elongated rods appeared in 3 days. Data were collected at 16 °C using a Rigaku RU-200 rotating anode X-ray generator operating at 55 kV and 85 mA and a Siemens multiwire area detector. Crystals of the DHPR−NADH−2,6-PDC complex typically measured 0.4 × 0.4 × 0.8 mm and diffracted to better than 2.2 Å. The unit cell parameters were determined on the basis of the auto-indexing function implemented in XDS (*24*). The crystals were orthorhombic with the pattern of systematically absent reflections consistent with space group $I222$ or $I2_12_12_1$. There is a dimer per asymmetric unit, and on the basis of molecular weight of 25 763 Da predicted from the deduced amino acid sequence, the value of V_m (*25*) is 2.63 Å^3/Da, which corresponds to a solvent volume fraction of 62%. The data were processed and reduced using SADIE and SAINT (*26*) and yielded the following final unit cell parameters: $a = 119.29$ Å, $b = 117.28$ Å, $c = 78.54$ Å, $\alpha = \beta = \gamma = 90.0°$. Crystals of the DHPR−NADPH−2,6-PDC complex typically measured 0.4 × 0.3 × 0.3 mm and diffracted to better than 2.4 Å. Data to 2.5 Å were integrated and reduced using XENGEN and yielded the following final unit cell parameters: $a = 118.83$ Å, $b = 118.26$ Å, $c = 79.38$ Å, $\alpha = \beta = \gamma = 90°$. Table 1 summarizes the data collection and processing statistics.

Structure Solution and Refinement. After several unsuccessful attempts to solve the structure of the *M. tuberculosis* DHPR−NADH−2,6-PDC complex in an orthorhombic body centered system using as a search model dimers generated from the *E. coli* DHPR monomer (*12*), a molecular replace-

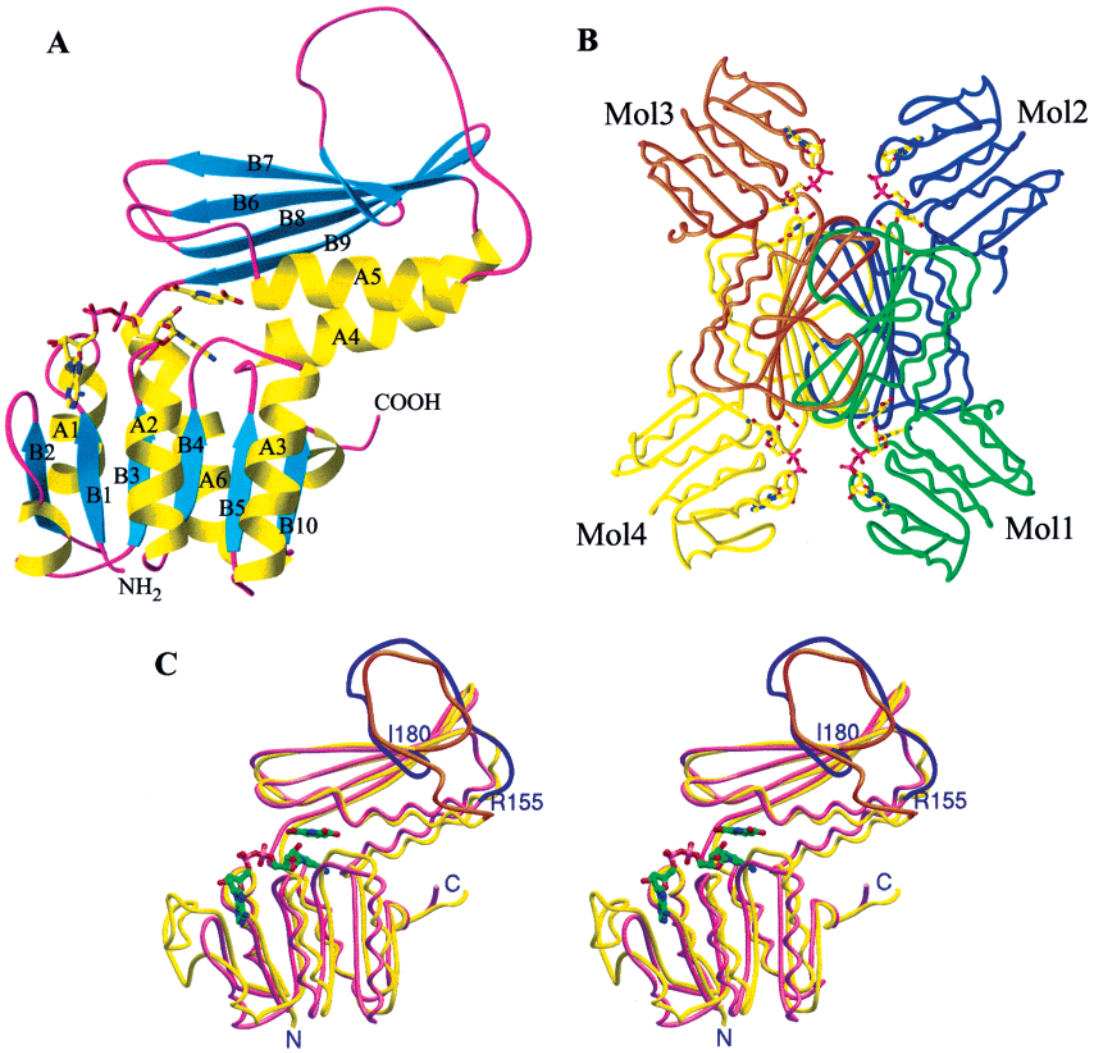

FIGURE 1: (A) Ribbon diagram of the *M. tuberculosis* dihydrodipicolinate reductase monomer with helices colored yellow and numbered consecutively and β strands colored blue and numbered consecutively. Bound NADH and 2,6-PDC are shown as ball-and-stick colored by atom type. (B) The *M. tuberculosis* dihydrodipicolinate reductase tetramer with each monomer individually colored. MOL1 and MOL2 represent the content of the asymmetric unit; MOL3 and MOL4 are generated by crystallographic symmetry. (C) Stereoview of the overlay of the Cα-traces of the *M. tuberculosis* (magenta) and *E. coli* (yellow) DHPR monomers. Bound NADH and 2,6-PDC are also shown as ball-and-stick. The loops connecting A5 to B7 in *M. tuberculosis* DHPR (residues Arg155-Ile180, dark blue) and A5 to B8 in *E. coli* DHPR (residues Leu182 to Ile206, orange) display a different topology: in both enzymes the loop starts and ends at almost the same place but proceeds in opposite directions (counterclockwise in *M. tuberculosis* DHPR, clockwise in *E. coli* DHPR). Although the direction of the loops are different, the role played by both in stabilizing the tetramer is essentially identical in the two structures. Figures 1 and 3 were generated using RIBBONS (*45*).

ment solution was found using an orthorhombic primitive space group and the *E. coli* DHPR tetramer as a search model. The rotation function was calculated using AMORE (*27*) between 12.0 and 4.5 Å and gave a single solution. The translation function was calculated using this rotation function and 9.0−4.5 Å data and gave a single solution. Multiple rounds of rigid body refinement and simulated annealing in X-PLOR (*28*, *29*) were used to obtain the initial electron density maps (see Supporting Information for a detailed description of the method used). The quality of the maps was very high, revealing side chains within the electron density envelope and density due to NADH and 2,6-PDC in all four subunits. At this point the dimer representing the asymmetric unit in the body centered system was identified, and the space group assigned as $I2_12_12_1$. All subsequent refinement was performed in this space group. The electron density was very poor for the long loop connecting α-helix 5 to β-strand 7 and α-helix 6 (Figure 1A), and these regions were omitted during initial stages of refinement. The resulting maps (both 2Fo−Fc and Fo−Fc) clearly showed that the loop was incorrectly oriented and that helix 6 was in a different position in the *M. tuberculosis* DHPR structure compared to the *E. coli* DHPR structure. This loop, helix 6, and two other regions (residues 33−46 and 227−245) were rebuilt manually, the entire sequence and side chains were assigned, NADH and 2,6-PDC were included, and the resolution was extended to 2.3 Å. Individual temperature factor refinement was included in the refinement strategy. Several water molecules were included in the model as were two PEG200 molecules, the latter included after finding 15 Å long, U-shaped positive electron density within the 16-stranded β-barrel tetramer interface. Extensive geometry checks were performed using WHAT_IF throughout the entire refinement, and the model was manually adjusted accordingly.

The structure of the DHPR−NADPH−2,6-PDC complex was solved by molecular replacement using the protein

portion of the *M. tuberculosis* DHPR−NADH−2,6-PDC complex as the starting model. Several rounds of model building in O and simulated annealing torsional refinement in XPLOR were used to adjust both main chain and side chain conformations. NADPH and 2,6-PDC were added when simulated annealing refinement converged to acceptable values of R and R_{free} (21.8 and 26.6%, respectively) using phases calculated from the protein alone. In the latter stages of refinement, both 2Fo−Fc and Fo−Fc maps were used to locate water molecules corresponding to positive density peaks having a value greater than 3σ. Table 1 summarizes the final refinement statistics for both models.

RESULTS AND DISCUSSION

Overall Structure of the Enzyme. The *Mycobacterium tuberculosis* dihydrodipicolinate reductase is a homotetramer composed of 245-residue monomers. Both structures reported here contain a dimer in the asymmetric unit, and the tetramer is generated by crystallographic symmetry. The R_{free} and R-factor for the NADH- and NADPH-containing ternary complexes are 25.0% and 24.3%, and 19.3% and 19.6%, respectively. Both models exhibit good geometry, and the Ramachandran plot (calculated with PROCHECK, 33) for the φ,ϕ angles reveal that all amino acid residues in both structures fall within the allowed regions of low conformational energy.

The *M. tuberculosis* DHPR monomer is shown as a ribbon diagram in Figure 1A. The root-mean-square deviation between identical Cα positions in the DHPR-2,6-PDC−NADH and −NADPH complexes is 0.4 Å, and we will discuss the overall fold using the NADH-containing structure. The monomer is composed of two domains, connected by two short hinge regions. The N-terminal domain is composed of residues Met1-Ala106 and Ser216-His245 and contains 6 β strands (B1−B5 and B10 in Figure 1A) and four α-helices (A1−A3 and A6 in Figure 1A) that form a structure reminiscent of a dinucleotide binding fold (*34*), but in which the two "halves" of this domain are different. The first half (Met1−Asp33) contains two β-strands and one α-helix and is connected to the second half by a loop that includes α-helix A1B (Leu38−Asp43). The second half (Val48−Ala102) contains three β-strands (B3−B5) and two α-helices (A2 and A3), with a fourth strand (B10) and additional helix (A6) contributed by the C-terminal residues (Ser216−Gly237). The topology of this fold is an unusual $+1x$, $-2x$, $-1x$, $-1x$ (*35*), similar to folds observed in flavodoxins (*36*, *37*), phosphoribosyltransferases (*38*−*41*), and *meso*-diaminopimelate dehydrogenase (*42*).

The C-terminal domain is the substrate and inhibitor binding domain and is formed by residues Leu107 through Ser211. This domain contains 4 β-strands (B6−B9 in Figure 1A) and two α-helices (A4 and A5 in Figure 1AA) that form an open, mixed α,β-sandwich (*35*). The C-terminal domain also has a long loop (Lys156−Gly179) that extends from the body of the monomer, at a 60° angle from this domain. The N- and C-terminal domains are connected by two short connections composed of Pro103−Ala106 (N > C) and Leu212−Thr215 (C > N) that function as hinges that allow for the movement of the two domains that accompany nucleotide and substrate binding (*12*, *13*).

The DHPR tetramer, the form present in solution, is generated from the dimer in the asymmetric unit by crystallographic symmetry (Figure 1B). The interactions between monomers in the tetramer are made exclusively by residues in the C-terminal domain. Two monomers in the asymmetric unit (Mol1 and Mol2 in Figure 1B) interact by pairing the four β-strands of the C-terminal domain to generate an 8-stranded mixed β-sheet. The 8-stranded sheets of two dimers (Mol1 + Mol2 and its symmetry mate, Mol3 + Mol4) pair face-to-face to generate a flattened 16-stranded β-barrel, anchored by B7, the outermost strand of each monomer, and the four long loops that extend from the core of the C-terminal domain. Each of these loops wraps around the four-stranded sheet of the neighboring monomer (Mol1 and Mol4, Mol2 and Mol3 in Figure 1B). Additionally, the core β-barrel is surrounding by 8 α-helices, two (A4 and A5) from each monomer. The A4 helices from adjacent monomers interact in an antiparallel fashion with an angle of 60° between their axes, as observed in other protein structures (*35*). The interior of the 16-stranded β-barrel contained two long, continuous areas of positive electron density (>3σ) that were modeled as molecules of poly(ethylene glycol) 200 ($C_8H_{18}O_5$, not shown).

The *E. coli* and *M. tuberculosis* dihydrodipicolinate reductases share only 29% sequence identity; yet their three-dimensional structures are very similar. The overlay of the Cα traces of the *M. tuberculosis* (magenta) and *E. coli* (yellow) reductase monomers is shown in Figure 1C. The root-mean-square deviation for 209 Cα atoms is 1.4 Å, with the major differences being the 22 amino acid-truncated N-terminal domain of the *M. tuberculosis* enzyme and the direction of the long loop in the C-terminal domain. The difference in the topology of the long loop is curious, since in both the *E. coli* and *M. tuberculosis* structures, the loop starts and ends at almost the same place (Figure 1C). In the *M. tuberculosis* structure, the loop begins at the end of A5 and proceeds in a counterclockwise manner until it connects with B7. In the *E. coli* structure, the loop similarly begins at the end of A5 but turns sharply and proceeds in a clockwise manner until it connects to B8, which is structurally equivalent to B7 in the *M. tuberculosis* structure. Although the direction of the loops are different, the role played by both in stabilizing the tetramer is essentially identical in the two structures.

Substrate and Inhibitor Binding Site. The substrate and inhibitor binding site on DHPR is located in the C-terminal domain in a region of extremely high sequence conservation (*12*). 2,6-PDC is a competitive inhibitor versus dihydrodipicolinate for the *E. coli* DHPR, exhibiting a K_i value of 26 μM (*10*). 2,6-PDC makes interactions with side chains of those amino acids that are highly conserved across bacterial species (Figure 2B). The aromatic ring of 2,6-PDC is stacked against the nicotinamide ring of bound NADH, with the position analogous to C4 of dihydrodipicolinate and the C4′ of bound nicotinamide (i.e., positions between which hydride transfer would occur) approximately 4 Å apart. The pyridine nitrogen atom is 3.2 Å away from the ϵ-amino group of Lys136, a group proposed to function in catalysis (*10*). Differences in the shape of the inhibitor binding pocket between the *E. coli* and *M. tuberculosis* DHPRs occur at the N-terminal end of B8 (B9 in the *E. coli* enzyme) and the nearby hinge region, generating a larger substrate/inhibitor binding site in *M. tuberculosis* DHPR.

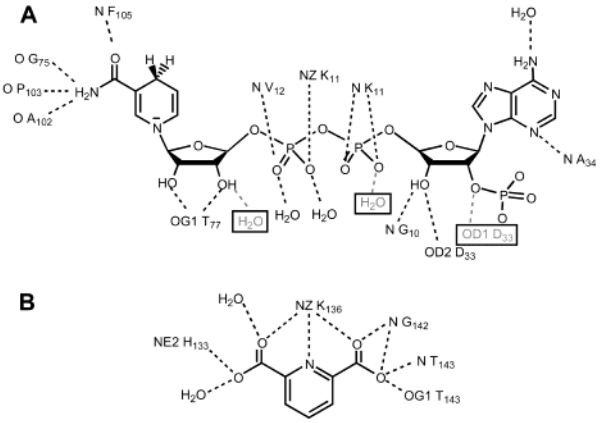

FIGURE 2: (A) Schematic diagram of the interactions between *M. tuberculosis* DHPR and NADPH. The boxed interactions are additionally observed in the NADH complex. (B) Interactions between *M. tuberculosis* DHPR and 2,6-pyridine dicarboxylate.

Pyridine Nucleotide Specificity among DHPR Orthologues. *E. coli* DHPR exhibits unusual nucleotide specificity, with NADH being bound more tightly (K_d = 0.46 μM) than NADPH (K_d = 2.1 μM) largely because of the large, negative entropic component to the free energy of NADPH binding (*10*, *14*). The dual specificity of *E. coli* DHPR was shown to result from the unusual presence of Glu38, shown to interact with both adenosyl ribose 2′- and 3′-hydroxyl groups of NADH, and the adjacent Arg39 residue, that interacts with the 2′-phosphate of NADPH (*14*). Sequence alignments (Table 2) of bacterial DHPR orthologues revealed differences in the pyridine nucleotide binding region between Gram-negative and Gram-positive and mycobacterial species. Sequences aligned from Gram-negative organisms contained both the acidic and basic residues that would predict dual specificity. Sequences aligned from Gram-positive organisms, archae, and mycobacteria contained only an acidic residue, and lacked any basic residues that might interact with the 2′-phosphate. This comparison suggested that the *M. tuberculosis* DHPR would exhibit a distinct preference for NADH compared to NADPH.

Surprisingly, the kinetic analysis revealed that the *M. tuberculosis* DHPR exhibits only a modest additional selectivity for NADH versus NADPH (Table 3, 6:1 based on relative V/K values, compared to 2:1 for the *E. coli* DHPR). In the *M. tuberculosis* DHPR−2,6-PDC−NADH and DHPR−2,6-PDC−NADPH complexes, both nucleotides are bound in an extended conformation across the C-terminal end of the N-terminal β-sheet and with the pyrophosphate moieties located directly over the "dinucleotide binding helix" (43, AI in Figure 1, Figure 3A). Both the adenosyl and nicotinamidyl ribose rings assume a C2′-endo conformation, and the adenine base is in an anti conformation. The numbers and types of hydrogen bonds formed between NADH and NADPH and the *M. tuberculosis* DHPR are very similar. In the NADH complex of *M. tuberculosis* DHPR, Asp33 (corresponding to Glu38 in the *E. coli* enzyme) makes hydrogen bond interactions with both the 2′- and 3′-hydroxyl groups of the adenosyl ribose ring. Alanine34 replaces the Arg39 residue of the *E. coli* enzyme, but Lys9 at the end of the β1 in the *M. tuberculosis* structure is positioned near, although pointed away from, the 2′- and 3′-hydroxyl groups of the adenosyl ribose. In the aligned sequences of bacterial DHPR's, a Lys or Arg residue is conserved among myco-

Table 2: Aligned Sequences of Bacterial Dihydrodipicolinate Reductases and NAD(P)H-Dependent Enzymes of Known Three-Dimensional Structure

Nucleotide Binding Sequence[a]	Organism (Accession Number)	(%Identity)	(%Similarity)[b]
[1]MRVGVL**G**A**K**G KV**G**ATMVRAV AAADDLTLSA EL**D**AGDPLSL[40]	*M. tuberculosis* (2498290)	(100%)	
[3]IKVGVL**G**AK**G** RV**G**QTIVAAV NESDDLELVA EIGVDDDLSL[43]	*C. glutamicum* (1169217)	(65%)	(76%)
[4]LRVAVL**G**AK**G** RI**G**SEAVRAV EAAEDMELVA ALGRGDGLEA[44]	*S. coelicolor* (7531086)	(61%)	(76%)
[2]IKVAVA**G**PR**G** KM**G**REAVKMI HEADTLELVA VVDSKHDGML[42]	*B. subtilis* (1706300)	(42%)	(57%)
[2]IRIAVV**G**AA**G** RM**G**KNLIEAV QQTGGAAGLT AAVDRPDSTL[42]	*P. aeruginosa* (12230904)	(33%)	(46%)
[18]IKVAVT**G**AL**G** RM**G**SNIIKTI TQQEDMKVVC AFEVPNHPKK[58]	*M. jannaschii* (7531267)	(30%)	(52%)
[6]IRVAIA**G**AG**G** RM**G**RQLIQAA LQMEGVALGA ALEREGSSLV[46]	*K. pneumoniae* (1169219)	(30%)	(50%)
[4]LKIAIA**G**AN**G** RM**G**RVLVEAV NNHPDTVLSG GALEHSGSEA[44]	*N. menigitis* (11252364)	(29%)	(45%)
[6]IRVAIA**G**AG**G** RM**G**RQLIQAA LALEGVQLGA AL**ER**EGSSLL[46]	*E. coli* (118242) (1ARZ.pdb)	(29%)	(44%)
[1]VRIAIA**G**AA**G** RM**G**RNLVKAT HQNPLSELGA GSERPESSLV[41]	*V. cholerae* (11252352)	(28%)	(43%)
[3]LKIAIA**G**AG**G** RM**G**CQLIQAV HSEAGVELGA AFERKGSSLV[43]	*H. influenzae* (1169218)	(25%)	(44%)
[168]ERVAVV**G**A**G**Y I**A**VELAGVIN GLGAKTHLFV **R**KHAPL**R**SFD	*E. coli* Glutathione reductase (1GET.pdb)		
[172]NHLVVV**G**G**G**Y I**G**LELGIAYR KLGAQVSVV**D** ARDRILPTYD	*P. putida* Lipoamide Dehydrogenase (1LVL.pdb)		
[177]LTVLVQ**G**L**G**A V**G**GSLASLAA EAGAQLLVA**D** TDTERVAHAV	*Rhodococcus* Phenylalanine Dehydrogenase (1CIC.pdb)		
[246]KTFAVQ**G**F**G**N V**G**LHSMRYLH RFGAKCVAVG **E**SDGSIWNPD	*Bovine* Glutamate Dehydrogenase (1HWX.pdb)		
[4]IRVAIV**G**Y**G**N L**G**RSVEKLIA KQPDMDLVGI FS**RR**ATLDTK	*C. glutamicum* Diaminopimelate Dehydrogenase (1DAP.pdb)		

[a] Emboldened residues constitute the GX(X)GXX(G/A) motif, while carboxy-terminal emboldened residues have been shown to interact with the adenosyl ribose 2′ and 3′ hydroxyls (**D** and **E**) or the 2′-phosphate (**R**). The underlined lysine residues (*K*) are those mutated to alanine in this study. [b] Determined using the Blast algorithm and the *M. tuberculosis* amino acid sequence as the search sequence.

Table 3: Kinetic Parameters Determined for WT, K9A, and K11A Mutant Forms of *M. Tuberculosis* Dihydrodipicolinate Reductase

	WT			K9A			K11A		
substrate	K_m (μM)	V_{rel}	V/K_{rel}	K_m (μM)	V_{rel}	V/K_{rel}	K_m (μM)	V_{rel}	V/K_{rel}
NADH	3.2 ± 0.4	100	100	2.5 ± 0.4	82	104	4.3 ± 0.9	276	206
NADPH	11.8 ± 1.5	62	16	42 ± 3	39	3.1	830 ± 150	288	1.1
$(V/K_{NADH})/(V/K_{NADPH})$			6.3			34			187

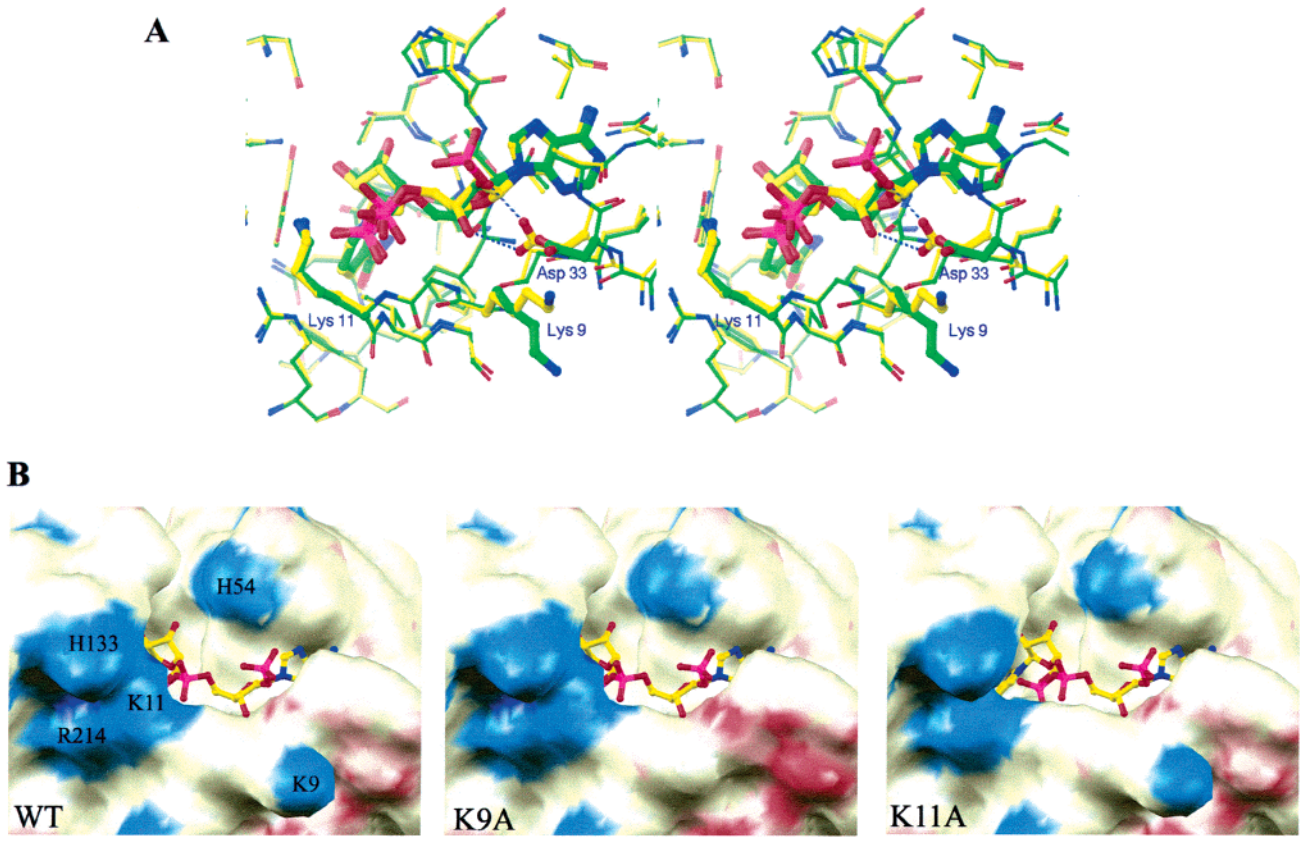

FIGURE 3: (A) Stereoview of the superimposed NADH and NADPH molecules at the active site of *M. tuberculosis* DHPR. The DHPR−NADH complex is colored with carbon atoms yellow, while the DHPR−NADPH complex is colored with carbon atoms green. (B) Grasp surface representations of the pyridine nucleotide binding region, showing bound NADPH, colored by atom type, in all cases. Left: WT *M. tuberculosis* DHPR. Middle: the K9A mutant form of *M. tuberculosis* DHPR. Right: the K11A mutant form of *M. tuberculosis* DHPR. Positive potential is colored blue with residue numbers indicated, and negative potential is colored red.

bacteria, corynebacteria, streptomyces and bacillus species (Table 3), but not in any Gram-negative bacteria. Mutation of this residue to Ala causes the nucleotide specificity to increase from 6:1 for the WT enzyme to 34:1 for the K9A mutant (Table 3). This is exclusively the result of a ca. 4-fold increase in the steady-state K_m value for NADPH, since the K_m value for NADH is statistically unchanged from its value for the WT enzyme in the K9A mutant.

A similar inspection of the nucleotide binding motif in the aligned DHPR sequences reveals a second cationic residue, K11 in the *M. tuberculosis* sequence, that is present as a basic residue in all bacterial DHPR's (Table 2). This residue, located at the beginning of the α1 helix of the β-α-β structural element (Figure 3A), is also near, and interacts with the pyrophosphate moiety. The other interactions with the pyrophosphate are hydrogen bonds to the main chain nitrogens of K11 and V12 (Figure 2A), and in other pyridine nucleotide binding enzymes, this residue is rarely basic (Table 2). Conversion of this single residue to an alanine residue has a number of dramatic, differential effects for NADH and NADPH. While the steady-state K_m value for NADH is essentially unaffected, the maximum velocity increases 2.7-fold, making this mutant a better enzyme than the WT enzyme. In the case of NADPH, the K_m value increases 70-fold, causing the nucleotide specificity ($V/K_{NADH}/V/K_{NADPH}$) to increase from 6:1 for the WT enzyme to 187:1 for the K11A mutant, a 30-fold change from this single substitution. In the structure of the NADPH complex, the negatively charged 2′-phosphate forces the carboxylate of Asp33 to move away from the phosphate (Figure 3). Although no direct contact between either K9 or K11 is observed in the structure, these two residues contribute to a highly positively charged environment in the region adjacent to the 2′-phosphate of NADPH (Figure 3B). We suggest that these two residues contribute to the binding of NADPH and consequently to the relaxed specificity for pyridine nucleotides.

On the basis of the conserved nature of cationic residues at this position in all bacterial DHPRases, we suggest that all these enzymes will exhibit the same degree of dual nucleotide specificity. *Mycobacterium tuberculosis*, like other organisms, maintain high $NADPH/NADP^+$ ratios and low $NADH/NAD^+$ ratios (*44*). Although most pyridine nucleotide-dependent enzymes exhibit a strong preference for NADH or NADPH, the ability to utilize the reducing equivalents in either reduced nucleotide pool would have obvious advantages for critical biosynthetic reactions under a number of physiological and metabolic conditions. Given the essential nature of the reaction catalyzed by DHPR to provide both *meso*-DAP and L-lysine, this may be an example of biological adaptation by gain of function. Finally, this region of the nucleotide binding motif has been hithertofore neglected as a determinant of nucleotide specificity, but might be considered in future protein engineering studies to modify nucleotide specificity by incorporating lysine residues into similar structural positions in NADH-dependent dehydrogenases and reductases.

CONCLUSIONS

Despite the relatively low degree of overall sequence identity, the *M. tuberculosis* and *E. coli* dihydrodipicolinate reductases share a high degree of structural homology. The regions that are most different are the N-terminal nucleotide binding domain where the deletion of twenty two residues results in a truncated, asymmetric "Rossmann" fold, and an unusual inversion in the orientation of a long loop involved in oligomer formation. The lack of a cationic residue known to be involved in contacts with the 2′-phosphate of bound NADPH in the *E. coli* enzyme suggested that the *M. tuberculosis* enzyme would exhibit higher steady-state affinity for NADH compared to NADPH. However, the *M. tuberculosis* enzyme exhibited only slightly diminished affinity for NADPH. Two residues that may compensate for the missing cationic residue were structurally identified and their role in enhancing NADPH binding demonstrated by site-directed mutagenesis.

SUPPORTING INFORMATION AVAILABLE

Figures and text regarding the solution, structures, and refinement. This material is available free of charge via the Internet at http://pubs.acs.org.

REFERENCES

1. Scapin, G., Blanchard, J. S. (1997) *Adv. Enzymol. Relat. Areas Mol. Biol. 72*, 279−324.
2. Kindler, S. H., and Gilvarg, C. (1960) J. *Biol. Chem. 235*, 3502−3512.
3. Berges, D. A., DeWolf, W. E., Dunn, G. L., Newman, S. J., Schmidt, J., Taggart, J., and Gilvarg, C. (1986) *J. Biol. Chem. 261*, 6160−6167.
4. Sundharas, G., and Gilvarg, C. (1967) *J. Biol. Chem. 242*, 3983−3984.
5. White, P. J. (1983) *J. Gen. Microbiol. 129*, 739−749.
6. Pavelka, M. S., and Jacobs, W. R., Jr. (1996) *J. Bacteriol. 178*, 644−6507.
7. Farkas, W., and Gilvarg, C. (1965) *J. Biol. Chem. 240*, 4717−4722.
8. Bouvier, J., Richaud, C., Richaud, F., Patte, J.-C., and Stragier, P. (1984) *J. Biol. Chem. 259*, 14829−14834.
9. Pavelka, M. S., Weisbrod, T. R., and Jacobs, W. R., Jr. (1997) *J. Bacteriol. 179*, 2777−2782.
10. Reddy, S. G., Sacchettini, J. C., and Blanchard, J. S. (1995) *Biochemistry 34*, 3492−3501.
11. Scapin, G., Blanchard, J. S., and Sacchettini, J. C. (1995) *Biochemistry 34*, 3502−3512.
12. Scapin, G., Reddy, S. G., Zheng, R., and Blanchard, J. S. (1997) *Biochemistry 36*, 15081−15088.
13. Wang, F., Blanchard, J. S., and Tang, X.-J. (1997) *Biochemistry 36*, 3755−3759.
14. Reddy, S. G., Scapin, G., and Blanchard, J. S. (1996) *Biochemistry 35*, 13294−13302.
15. Wierenga, R. K., Terpstra, P., and Hol, W. G. J. (1986) *J. Mol. Biol. 187*, 101−107.
16. Scrutton, N. S., Berry, A., and Perham, R. N. (1990) *Nature 343*, 38−43.
17. Baker, P. J., Britton, K. L., Rice, D. W., Rob, A., and Stillamn, T. J. (1992) *J. Mol. Biol. 228*, 662−671.
18. Hurley, J. H., and Dean A. M. (1994) *Structure 2*, 1007−1016.
19. Karplus, P. A., and Schulz, G. E. (1989) *J. Mol. Biol. 210*, 263−180.
20. Bystroff, C., Oatley, S. J., and Kraut, J. (1990) *Biochemistry 29*, 3263−3277.
21. Sem, D. S., and Kasper, C. B. (1993) *Biochemistry 32*, 11548−11558.
22. Ho, S. N., Hunt, H. D., Horton, R. M., Pullen, J. K., and Pease, L. R. (1989) *Gene 77*, 51−59.
23. Sanger, F., Nicklen, S., and Coulson, A. R. (1977) *Proc. Natl. Acad. Sci. U.S.A. 74*, 5463−5467.
24. Kabsch, W. (1988) *J. Appl. Crystallogr. 21*, 916−924.
25. Matthews, B. (1968) *J. Mol. Biol. 33*, 491−497.
26. *SAINT version 4 Software Reference Manual* (1996) Siemens Industrial Automation, Inc., Madison, WI.
27. Navaza, J. (1994) *Acta Crystallogr. A50*, 157−163.
28. Brunger, A. T., Kuriyan, J., and Karplus, M. (1987) *Science 235*, 458−460.
29. Brunger, A. T., Krukowski, J., and Erickson, J. (1990) *Acta Crystallogr. A46*, 585−593.
30. Brunger, A. T. (1992) *Nature 355*, 472−474.
31. Read, R. J. (1986) *Acta Crystallogr. A42*, 140−149.
32. Jones, A. T., Zuo, J. Y., Cowan, S. W., and Kjeldgaard, M. (1991) *Acta Crystallogr. A47*, 110−119.
33. Laskoswski, R. A., MacArthur, M. W., Moss, S. D., and Thorton, J. M. (1993) *J. Appl. Crystallogr. 26*, 283−291.
34. Rossmann, M. G., Lilijas, A., Branden, C.-I., and Banaszak, L. J. (1975) *Enzymes*, 3rd ed., *11*A, 61−102.
35. Richardson, J. S. (1981) *Adv. Protein Chem. 34*, 167−339.
36. Watenpaugh, K. D., Sieker, L. C., and Jensen, L. H. (1973) P*roc. Natl. Acad. Sci. U.S.A. 70*, 3857−3860.
37. Burnett, R. M., Darling, G. D., Kendall, D. S., LeQuesene, M. E., Mayhew, S. G., Smith, W. W., and Ludwig, M. L. (1974) *J. Biol. Chem. 249*, 4383−4392.
38. Scapin, G., Grubmeyer, C., and Sacchettini, J. C. (1994) *Biochemistry 33*, 1287−1294.
39. Smith, J. L., Zelulec, J., Warey, J. J.-P., Niu, L., Switzer, R. L., Zlakin, H., and Setow, Y. (1994) *Science 264*, 1427−1433.
40. Eads, J. C., Scapin, G., Xu, Y. Grubmeyer, C., and Sacchettini, J. C. (1994) *Cell 78*, 325−334.
41. Somoza, J. R., Chin, M. S., Focia, P. J., Wang, C. C., and Fletterick, R. J. (1996) *Biochemistry 35*, 7032−7040.
42. Scapin, G., Reddy, S. G., and Blanchard, J. S. (1996) *Biochemistry 35*, 13540−13551.
43. Vos, S., deJersey, J., and Martin, J. L. (1997) *Biochemistry 36*, 4125−4134.
44. Gopinathan, K. P., Sirsi, M., and Ramakrishnan, T. (1963) *Biochem. J. 87*, 444−448.
45. Carson, M. (1997) *Methods Enzymol. 277*, 493−505.

BI030044V